arXiv:astro-ph/0604411v1 19 Apr 2006

Precision Measurement of Optical Pulsation using a Cherenkov Telescope

J. A. Hinton [a,b,*] , G. Hermann [a] , P. Krötz [a,c] , S. Funk [a]

[a] *Max-Planck-Institut für Kernphysik, P.O. Box 103980, D-69029 Heidelberg, Germany*

[b] *Landessternwarte, Königstuhl, D-69117 Heidelberg, Germany*

[c] *now at: Physikalisches Institut, Universität zu Köln, Germany*

Abstract

During 2003, a camera designed to measure the optical pulsations of pulsars was installed on a telescope of the H.E.S.S. array. The array is designed for γ-ray astronomy in the $\sim$ 100 GeV - 100 TeV energy regime. The aims of this exercise were two-fold: to prove the pulsar timing capabilities of H.E.S.S. on all relevant time-scales, and to explore the possibility of performing sensitive optical pulsar measurements using the $\sim$ 100 m^2 mirror of a Cherenkov telescope. Measurements of the Crab pulsar with this instrument demonstrate an order of magnitude sensitivity improvement over previous attempts using Cherenkov telescopes. Here we describe the design and performance of the system and discuss design considerations for future instruments of this type.

Key words:
PACS: 97.60.Gb, 95.85.Kr
Crab pulsar, optical pulsations, Cherenkov telescopes

1 Introduction

The six nearby high spin-down luminosity pulsars known at γ-ray energies provide a laboratory for the study of high energy processes under extreme conditions [1]. The extremely strong gravitational and magnetic fields close to pulsars make the modelling of such objects rather complex. Indeed, the acceleration processes at work in pulsar magnetospheres, and the associated

* Corresponding author, Jim.Hinton@mpi-hd.mpg.de

broad-band non-thermal *pulsed* emission, remain poorly understood despite several decades of effort. Observations in a wide range of wavelength bands are required to provide information not just on different particle energies, but also on different regions within the magnetosphere. Observations above 10 GeV are widely seen as key to our understanding of the origin of the high energy emission (see for example [2,3]). A small number of (apparently pulsed) photons above this energy were detected by the EGRET satellite but statistics were insufficient to extend pulsed spectra much beyond 10 GeV [4]. The much larger collection area of ground based instruments is required to explore the very high energy (VHE) regime. The major new air-Cherenkov experiments for ground based γ-ray astronomy, such as H.E.S.S. [5], MAGIC [6] and VERITAS [7] exhibit greatly improved sensitivity around 100 GeV compared to previous instruments [8,9]. Detections or upper limits on pulsed emission from these new instruments will likely be based on data taken over months or even years. Especially in the case of non-detection of a pulsed signal, it is necessary to prove the long term stability and accuracy of the timing systems of the experiment. The key components of the timing system are the timing hardware (usually based on GPS clock technology), with associated interface electronics, and the software used to derive phase information for an individual object. Some of these γ-ray pulsars exhibit pulsed emission detectable at optical wavelengths. The detection of pulsed optical emission using the timing system of a γ-ray instrument can be used as a means to demonstrate its absolute timing capability.

Optical pulsar measurements are also interesting in their own right (see for example [10]). The six known optical pulsars exhibit dominantly non-thermal (optical) emission and are all relatively young, and energetic or nearby. The class of pulsars with measured optical pulsations therefore falls close to the class of potential very-high-energy γ-ray emitting pulsars. The optical emission also provides a bridge between the well studied radio and X-ray bands. The recent claim of enhanced optical emission associated with giant radio pulses (GRPs) of the Crab pulsar [11], acts as an additional motivation for further studies.

Optical observations of pulsars using conventional optical telescopes are performed either with fast readout CCD cameras [12] or photon counting instruments [13]. The requirements for such a device are time-resolution of $\sim$100 μs and sufficient signal/noise to resolve the pulsed emission against the night sky background (NSB). Sensitivity improves linearly with both optical PSF width and mirror diameter. Traditional devices have excellent angular resolution and modest mirror area. An alternate concept is to use the large mirror area of Cherenkov telescopes to compensate for their modest angular resolution. The potential advantages of this approach include smaller fluctuations due to *seeing* (intensity fluctuations on small angular scales caused be atmospheric turbulence), potentially deadtime free operation and in general a

different set of systematic effects. The idea of measuring the optical pulsations of pulsars with Cherenkov telescopes is at least a decade old and pulses from the Crab pulsar have been measured successfully by several instruments: Whipple [14], STACEE [15], CELESTE [9], and HEGRA [16], with a typical sensitivity of $0.1\,\sigma/\sqrt{t/\mathrm{s}}$ (i.e. a one second observation leads on average to an 0.1 standard deviation detection significance, increasing with the square-root of time, t). The most recent measurement, using the modestly sized (1.7 m diameter) mirror of the HEGRA CT-1 telescope, is described in [16]. This measurement achieved a sensitivity of $0.14\,\sigma/\sqrt{t/\mathrm{s}}$ and the authors estimate a value of $1\,\sigma/\sqrt{t/\mathrm{s}}$ can be achieved for the MAGIC telescope using the same device (indeed a preliminary study using MAGIC [17] confirms this predicted sensitivity. However, as all other known optical pulsars are dimmer than the Crab by a factor > 200, even with this level of sensitivity over 600 hours of observations would be required to detect pulses from any pulsar apart from the Crab.

The advantage of the H.E.S.S. telescopes (15 m focal length, 107 m^2 of reflector) is that the optical point spread function is considerably smaller than the pixel size for on-axis observations, with a FWHM of only 0.07°[18,19]. To exploit this advantage a single-channel prototype system was installed on the first H.E.S.S. telescope for 8 nights of Crab pulsar observations in January 2003 [20]. A 7-pixel optical pulsar camera with improved electronic and optical properties was installed in October 2003 on the last of the H.E.S.S. telescopes to receive a Cherenkov camera. The observations described here were performed with this new camera during October and November 2003.

2 The Camera System

The main improvement over the (single-channel) prototype device described in [20] is the addition of a 6 channel "veto" camera surrounding the central pixel. The additional channels have the dual purpose of identifying optical atmospheric transients such as air-showers and meteorites, and of monitoring the NSB level close to the target pulsar. The optical pulsar camera is shown in figure 1. The camera box contains seven photomultiplier tubes (PMTs) with associated light cones, a high voltage distribution system and two positioning LEDs. The Photonis XP2960 PMTs and the light collecting cones are the same as used for the H.E.S.S. Cherenkov camera [21]. The wavelength dependence of the instrument response is given in figure 2. The central pixel is equipped with an exchangeable aperture (of 1 to 22 mm diameter). 20 or 22 mm apertures were used for most of the data discussed here, providing optimal signal to noise given the on-axis optical point-spread-function of a H.E.S.S. telescope at 46° zenith angle (the culmination of the Crab). The 1 mm (pin-hole) aper-

ture is used for pointing tests using stars. The camera box is equipped with a pneumatic lid. The positioning LEDs are used to monitor pointing and tracking accuracy via images acquired by a CCD camera mounted at the centre of the telescope dish, with the pulsar camera in its field of view.

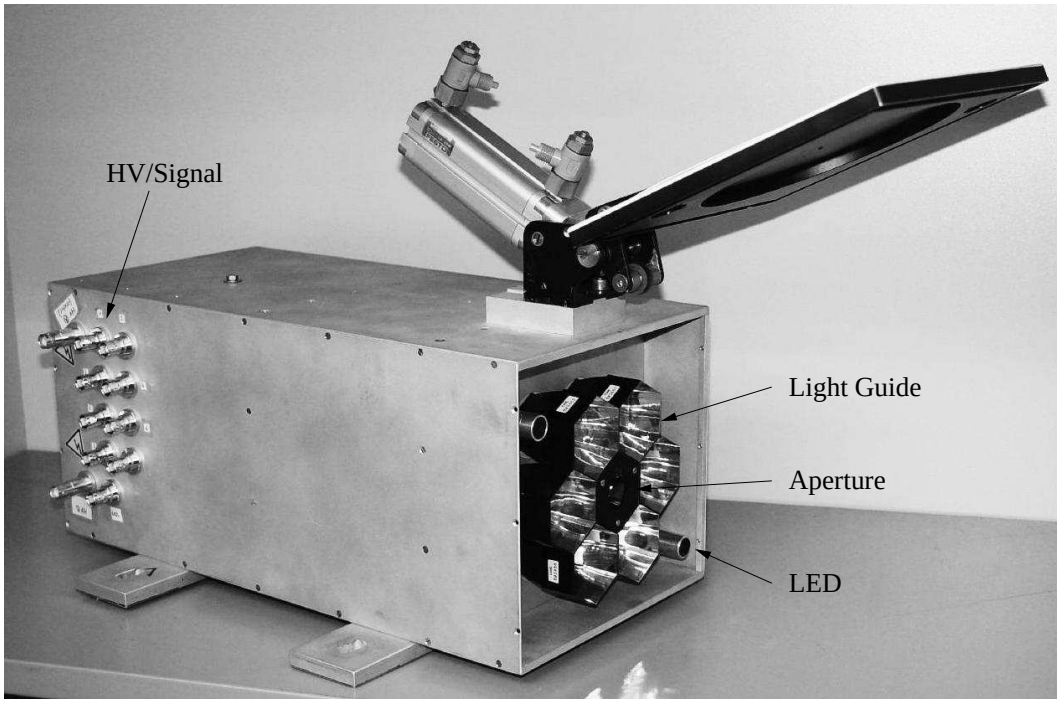

Fig. 1. Photograph showing the principle mechanical components of the optical pulsar camera: the central pixel aperture, the "veto" pixel light guides, the positioning LEDs and the HV inputs/signal outputs for the photomultipliers mounted within the casing.

The analogue signals from the seven camera pixels were fed via 50 m coaxial cables to an electronics container at the base of the telescope. The camera electronics were housed in this temperature controlled environment. Signals from all channels were amplified with DC-coupled spectroscopic shaper modules, with a characteristic shaping time of 100 μs (FWHM). The signal was then digitised with an over-sampling factor of $\sim$ 4 using a HYTEC VTR 2536 14-bit Flash ADC. This scheme provides a current measurement proportional to the average photon flux on 100 μs time-scales. Any optical pulsed signal is measured on top of a DC background generated by NSB photons, which have a typical rate of $\sim$100 MHz.

Timing information was provided by two Meinberg 167BGT GPS clocks, one associated with the H.E.S.S. central trigger system [22] and a second identical clock housed on the telescope tracking room. These clocks supply 10 MHz and 1 Hz TTL outputs synchronized to UTC. For the H.E.S.S. clock these signals were distributed via optical fibre from the central control building. Two VME counter models are used to count these TTL pulses and generate

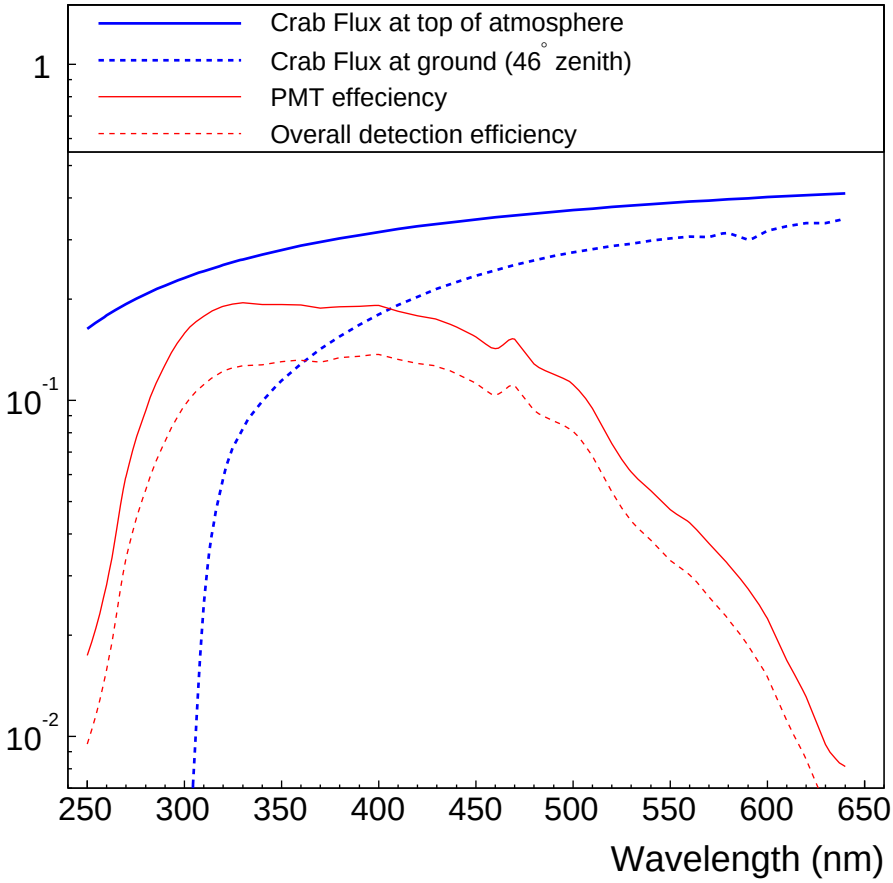

Fig. 2. Wavelength dependent efficiency of the instrument compared to the optical spectrum of the Crab nebula [28], before and after atmospheric absorption. The lower solid curve gives the combined quantum and collection efficiency of the PMT. The dashed curve includes also the reflectivity of the primary mirror and the overall collection efficiency of the light cone.

event timestamps. The 1 Hz channel is used to reset the 10 MHz counter. Every two seconds an ASCII time-string was read via a serial port on the GPS clock, as an absolute time reference. The clock counters are read out together with each FADC sample via a VME based CPU. A custom data acquisition system (DAQ) developed for this measurement achieved the required over-sampling factor of $\sim$4 with an average sampling rate 28 kHz on all channels. Additional electronics in the electronics container provided temperature monitoring and remote control of photomultiplier HV and the camera lid. Data transmission to a remote machine responsible for data storage occurred in parallel to data taking — resulting in deadtime free operation. Due to the large sampling rate the pulsar camera produced data at a rate comparable with that of the H.E.S.S. 960 pixel Cherenkov cameras ($\sim$1 MB/s).

3 Observations

The observations described here were performed in late October and early November 2003, partly contemporaneous with observations using the Effelsberg 100 m radio telescope (discussed in [23]). The optical measurements described here were accompanied by γ-ray observations of the Crab nebula with the 3 remaining H.E.S.S. telescopes. Overall 60 hours of optical Crab observations were performed of which 41 hours of on-source observations pass all data quality criteria. Over 300 GB of raw data were obtained.

The observations consisted of data taken tracking the Crab pulsar itself, interspersed with occasional off-source runs and periodic pedestal monitoring runs taken with the camera lid closed. Observations occurred semi-automatically, with intervention from the H.E.S.S. shift-crew only at the beginning and end of each night. To keep the camera centred on the pulsar it was necessary to make online corrections for atmospheric refraction and bending in the arms of the telescope. The verification of the absolute pointing of the instrument was done by scanning several stars across the aperture of the central pixel, and also using CCD images of the positioning LEDs and star images on the camera lid. The telescope tracking precision was monitored during the measurement and exhibited a maximum rms deviation of 3 $''$. The total systematic pointing error is estimated as $\sim 30''$, introducing a negligible error on the recorded optical signal.

For roughly half of the observing time, two independent GPS clocks were readout in parallel: the H.E.S.S. central trigger timing system and the independent system of the optical pulsar instrument. The mean difference between the two event time-stamps during this time was 2.1 μs, consistent with the length of the optical fibre over which the central clock time was transmitted. The rms of this time difference was 150 ns, consistent with the precision quoted by the clock manufacturers.

The night sky background level in the camera FOV is rather inhomogeneous. The Crab nebula has a V-band magnitude of 8.4 and a diameter of $\approx 6'$, covering essentially the entire central pixel. The brightest star present in the surrounding pixels has $M_{\rm v} = 9.9$, causing significant variation in pixel currents as it rotates around the outer pixels. The mean NSB level in the outer pixels was found to be of $\sim 3 \times 10^{12}$ photons m^{-2} s^{-1} sr^{-1}. Previous measurements of the NSB level at the H.E.S.S. site found $\approx 2.4 \times 10^{12}$ photons m^{-2} s^{-1} sr^{-1} (300-650 nm) close to the zenith and levels higher by a factor $\sim$ 2 on the galactic plane in the outer galaxy [29]. NSB measurements of this field using a HEGRA telescope on La Palma [16] yielded a value of 4.3×10^{12} photons m^{-2} s^{-1} sr^{-1}, in reasonable agreement, given the different site and the different altitude range of our observations.

4 Analysis & Results

The first step of the analysis is the summation of every four consecutive samples to produce statistically independent measurements of $\approx 140\,\mu$s duration. A timestamp is generated based on the average time of the four samples. For each five minute observation run, pedestal values are subtracted based on the ADC values with the camera lid closed. Periods with unstable weather conditions are removed by cuts on the rms and gradient in the signals measured in the veto pixels. Transient background events are removed by excluding 2 s blocks in which the signal in any *surrounding* pixel exceeded 5 times the signal rms for any 5 consecutive measurements. No cuts are made based on the central pixel signal.

4.1 Timing and Light-Curve

A crucial aspect of the analysis is the barycentering and phase-folding of the event times. For this purpose software developed specifically for H.E.S.S. was employed [24]. The software has been compared against the standard TEMPO package [25,26] and no difference greater than 1 μs found for non-binary pulsars. Ephemerides from Jodrell Bank were used for the phase calculation [27]. Comparing the ephemerides provided for October and November we derive a second derivative of the pulsar frequency: $\ddot{f} = 9.3 \times 10^{-21}\,\mathrm{s}^{-3}$. This value of $\ddot{f}$, together with $\dot{f}$, f and t_0 taken from the published November 15^{th} ephemerides, was used to calculate the absolute phase information given here.

Following phase-folding a clear signal from the Crab pulsar was visible in all datasets. The average signal/noise of the full dataset is such that an average significance of $4\,\sigma/\sqrt{t/\mathrm{s}}$ can be assigned to the pulsed signal, more than an order of magnitude better than previous Cherenkov telescope measurements. The level of precision achievable on different time-scales is illustrated in figure 3. Phase-folded light-curves extracted from 10 s, 100 s and 1 hour datasets are shown. Even in a 10 s exposure, the peak position is resolved (inset in figure 3) to better than 1 ms. The position of the peak in subsets of the data is determined by a fit of a smoothed version of the overall measured phasogram with two free parameters: the normalisation and the relative phase shift. This empirical fit function is shown in the inset of figure 3.

As can be seen from figure 4 the position of the main peak can be measured with an accuracy of $< 20\,\mu$s in one 5-minute run. Unfortunately the available radio ephemerides have an absolute precision of $\sim 70\mu$s, so any comparison is limited by the radio accuracy. The apparent drift during the period of our measurements ($\sim$ one month) was $\approx$60 μs, consistent within the accuracy of

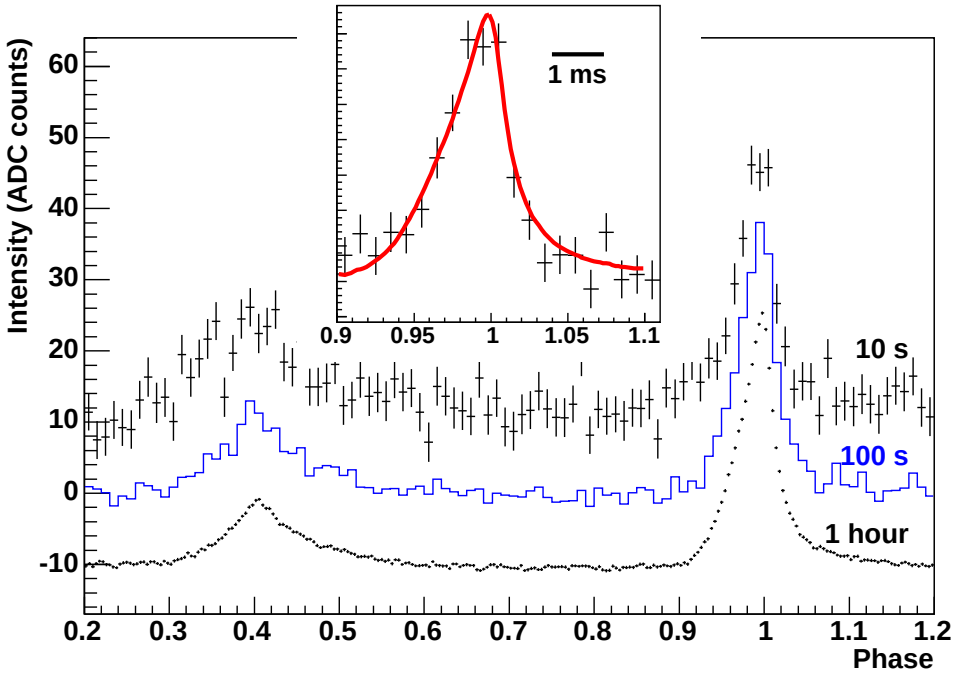

Fig. 3. Average optical signal versus phase for the Crab pulsar for 10 second, 100 second and 1 hour integration times. The inset shows a fit to the main peak for the 10 second dataset. For clarity, offsets of ±10 counts have been added to the 10 s and 1 h datasets. The DC signal produced by the Crab nebula and the NSB has been subtracted ($\sim 2 \times 10^4$ ADC counts).

the Jodrell ephemerides for October and November. The apparent phase shift of the mean peak between January and November 2003 was ≈100 μs, again consistent within the accuracy of the radio ephemerides used.

The phasogram extracted from the full 39 hour dataset is shown in figure 5. The best published optical phasogram for the Crab nebula is that extracted from 2 hours of observations with the Hubble Space Telescope (HST) [28]. We find generally good agreement between the H.E.S.S. result and that of HST. For example, the ratio of the height of the main pulse to that of the inter-pulse: HST 3.78±0.11, H.E.S.S. 3.721±0.003; and the FWHM of the main peak: HST 0.0431±0.0003, H.E.S.S. 0.0445±0.0001. The H.E.S.S. measurement is 40 μs wider than that from HST, consistent with the expected smearing introduced by imperfect ephemerides over the long exposure time. Indeed, fits to all 489 individual 5 minute phasograms show a mean value of 0.0432±0.0001, identical to the HST result. In our data the phase position of the main optical pulse precedes that of the radio peak by 134±2 μs, again consistent with previous measurements (100 μs [11]) within the error introduced by the imperfect radio ephemeris.

The signal measured with our instrument corresponds approximately to the

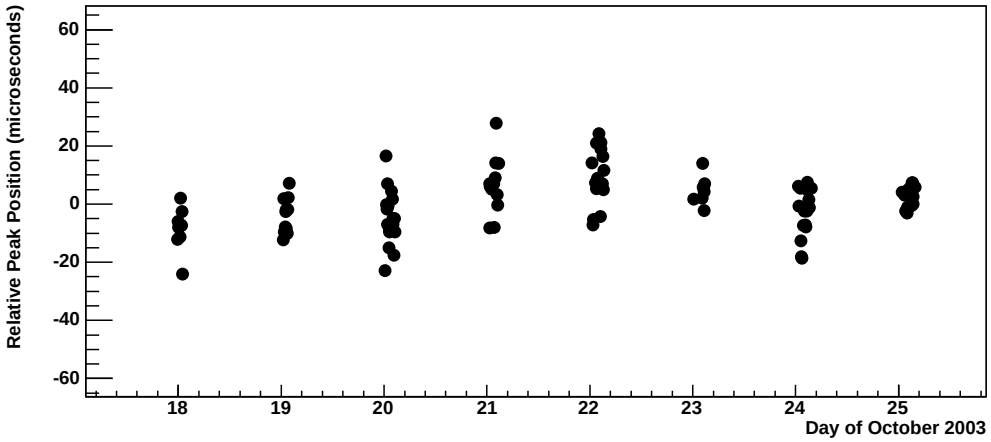

Fig. 4. Reconstructed relative main peak position for the Crab pulsar over one week in October 2003. Each point represents one 5 minute run.

wavelength range 300-650 nm, with a rather non-uniform response illustrated in figure 2 (more details on the individual optical components can be found in [18]). The most meaningful way to compare the pulsed flux measured here with previous measurements is to convolve the measured Crab pulsed spectrum with our wavelength dependent response function. Using the spectrum reconstructed by [28] we predict a pulsed signal of 1000 photoelectrons per pulse (at 46° zenith). The mean measured value is 1200 p.e./pulse, in good agreement within the ≈30% systematic error introduced by uncertainties in instrumental reflectivities, efficiencies and atmospheric transmission.

4.2 Search for Giant Pulses

Extreme pulse height variability is a common feature of radio pulsars. Giant radio pulses (GRPs) are normally coincident with main pulse and inter-pulse [11] but can apparently also occur in other phase regions [23]. While an analogous phenomenon has not so far been seen in the optical, an average 3% enhancement in flux of the optical pulse, in coincidence with GRPs, has been reported [11]. Given the signal/noise of our measurement a few $\times 10^4$ simultaneous GRPs would be required to confirm this value. However, given the relatively long duration of our measurement it is useful to derive a limit on the rate of *large* optical pulses, independent of the radio pulse height.

The major background for such a search in our dataset is meteorites. These are normally detected in several pixels and take ≈50 ms to cross the camera. Such events, as for example that shown in figure 6, are readily rejected from the

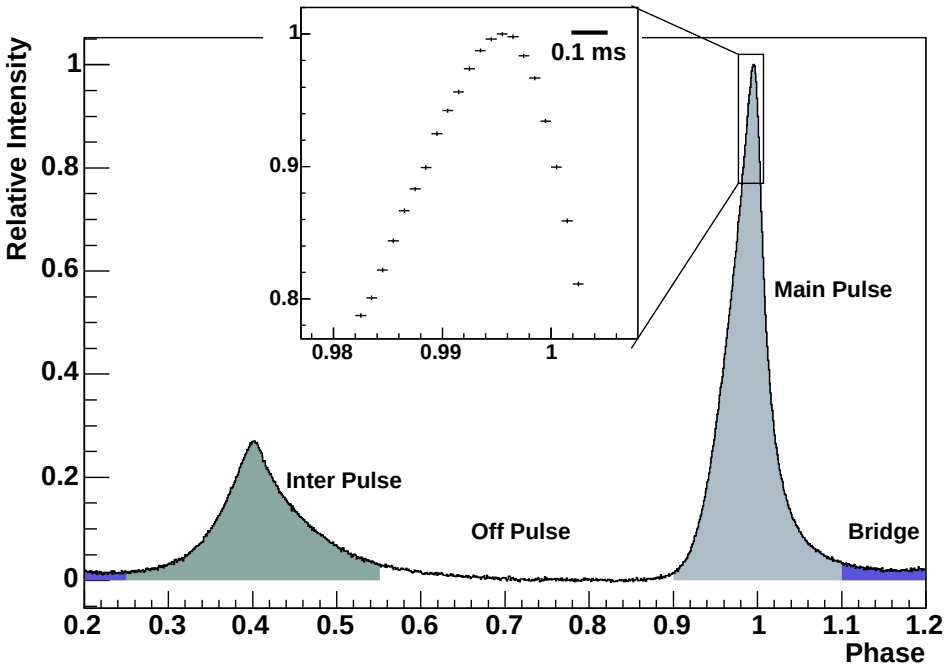

Fig. 5. Phasogram extracted from the complete 39 hour dataset. The main phase regions are marked: the bridge emission (0.1-0.25), the inter-pulse (0.25-0.55), the main pulse (0.9-1.1) and the off pulse region (0.55-0.9). The inset shows the 3% of the phase around the main peak position on an expanded scale. The 100 μs scale bar in the inset corresponds to the shaping time of the measurement, any structures in the light-curve on shorter timescales are unresolvable.

analysis using the outer pixel information. However, an irreducible background of events travelling almost on-axis and hence illuminating only the centre pixel, is present. Figure 7 shows the distribution of integrated signal in each pulse (or on- and off- phase regions) normalised by the expected poisson fluctuations. No fluctuations $> 20\times$ the mean pulse amplitude were observed during our measurement, neither on- nor off-phase. We can therefore place a limit on the fraction of such large pulses of 1.4×10^{-6} (95% confidence). This result should be compared to the situation at radio frequencies where pulses exceeding the mean flux by several orders of magnitude are frequent. We note that our instrument is sensitive to giant pulses of very short (< 1 μs) duration, as seen in the radio band, which may not be the case for photon counting instruments.

5 Summary and Outlook

We have constructed and tested an optical pulsar monitoring system for installation on Cherenkov telescopes. We have shown that such a system can approach the sensitivity of conventional optical telescopes (with custom built

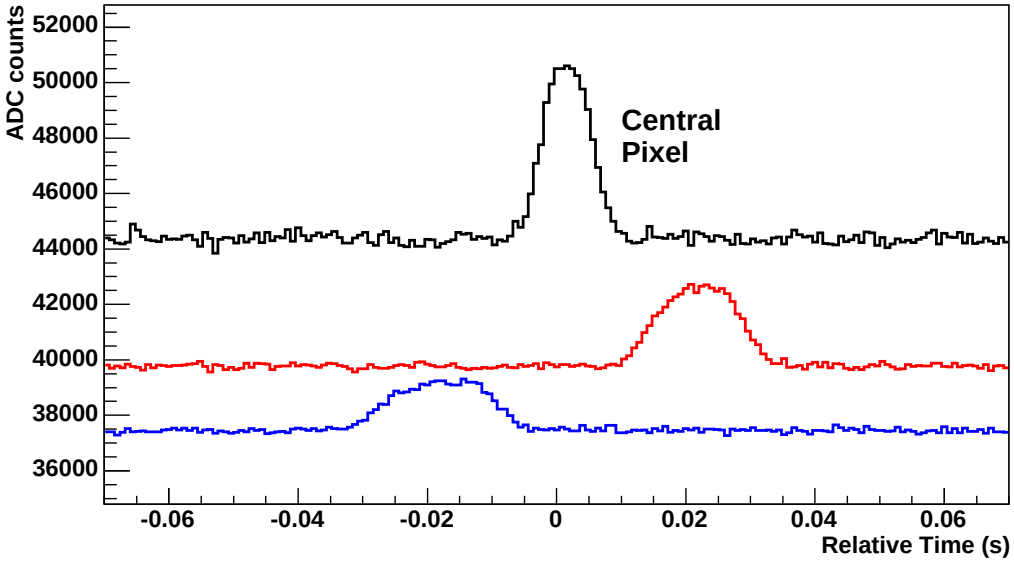

Fig. 6. Light-curve in three pixels indicating the passage of a meteorite candidate. The central pixel (upper curve) shows a narrower profile than that of the outer pixels (lower curves) due to its reduced aperture.

cameras) in measuring short-time-scale (millisecond-second) optical pulsations. In addition, the excellent agreement on the shape of the Crab pulsar light-curve validates the timing hardware and software used for H.E.S.S., thus demonstrating the validity of pulsed emission limits from H.E.S.S [30]. We also derive an upper limit on the frequency of *giant pulses* which is complementary to existing limits and measurements in that it includes also very short ($\sim$ nanosecond) pulses.

As the energy threshold of the IACT technique are pushed down further (e.g. with the second phases of both the H.E.S.S. and MAGIC experiments), the detection of pulsed VHE γ-ray emission will become more likely, thereby increasing the importance of optical monitoring devices. We consider two possibilities for future instruments of this type. Firstly a small device for monitoring purposes, gathering data in parallel to γ-ray with the Cherenkov camera. Ideally such an instrument would replace one pixel of the Cherenkov camera. The problem with this approach is the observing strategy of modern instruments, for example 'wobble' mode and convergent pointing, both of which move the target source away from the centre of the field of view of the telescopes. Field rotation then prevents the observation of a source in a signal pixel through an entire run. The second possibility is to adapt the photo-sensor current monitoring of a Cherenkov camera to provide high rate (>1 kHz) and resolution sampling of the sky brightness. With integration and sampling rates on comparable time scales such a camera could be used to measure optical pulsations (and transients) anywhere in the $\sim 4^\circ$ field of view of the instrument, in par-

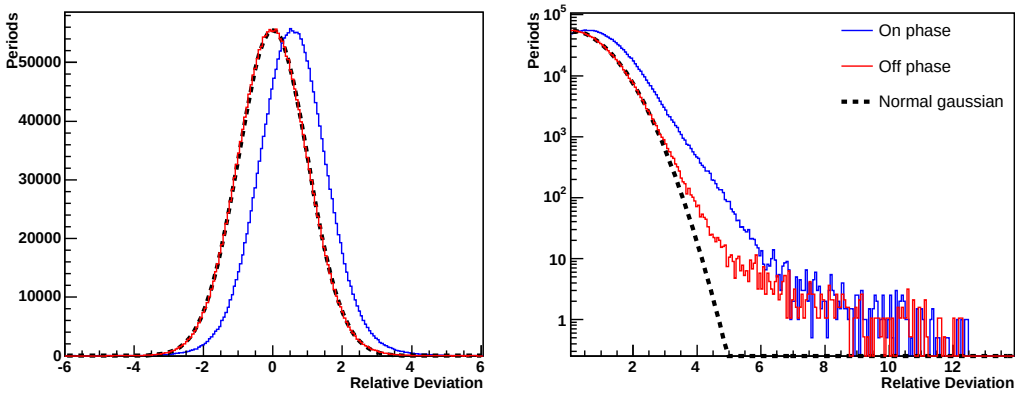

Fig. 7. Relative fluctuations in the integrated signal in on- and off-phase regions for each pulse (linear scale - left and log. scale - right). The on-phase region corresponds to the main pulse and inter-pulse regions shown in figure 5. Off-pulse here corresponds to a combination of the true off-pulse region and the bridge region as shown in figure 5. After tight quality selection to remove optical transients and unstable weather, 2.2 million pulses remain. The off-phase distribution follows closely a normal gaussian distribution (dashed-line) as expected, but with a significant tail to large values. This tail can be attributed to transient events occurring only in the central pixel. A similar tail is seen on the on-phase distribution.

allel to γ-ray observations. A camera with these properties is currently under test [31]. For the 600 m^2 class telescopes of the next generation, deep observations of young pulsars with such a system could lead to the discovery of new optical counterparts to known radio pulsars. Such a system is also desirable in the search for MeV/GeV emission from short time-scale GRBs [32].

Acknowledgements

The authors would like to acknowledge the support of their host institutions, and additionally support from the German Ministry for Education and Research (BMBF). We appreciate the excellent work of the engineering and technical support staff in Heidelberg and Namibia in the construction and operation of the equipment. We would like to thank the entire H.E.S.S. collaboration for their cooperation and assistance, in particular: F. Breitling, K. Bernlöhr, O. Bolz, S. Gillessen, M. Holleran.

References

[1] Nolan, P.L., *et al.*, 1996, Astron. Astrophys. Suppl. Ser. **120**, 61.

[2] Daugherty, J.K. & Harding, A. K., 1982, ApJ **252**, 337.

[3] Hirotani, K., 2001, ApJ **549**, 495.

[4] Thompson, D. J. *et al.*, 2005, ApJ Suppl., **157**, 324.

[5] Hinton, J.A., 2004, New Astron. Rev. **48**, 331.

[6] Lorenz, E., 2004, New Astron. Rev. **48**, 339.

[7] Weekes, T.C. *et al.*, 2002, Astropart. Phys. **17**, 221.

[8] Hanna, D. S., *et al.*, 2002, Nucl. Inst. & Methods **A491**, 126.

[9] de Naurois, M., *et al.*, 2002, ApJ **566**, 343.

[10] Shearer, A. & Golden. A, 2002, in *Neutron stars, Pulsars and Supernova remnants*, eds W. Becker, H. Lesch & W. Trümper, MPE report 278, p. 44-53 (astro-ph/0208579)

[11] Shearer, A., *et al.*, 2003, Science **301**, 493.

[12] Dhillon, V. & Marsh, T., 2001, New Astron. Rev. **45**, 91.

[13] Straubmeier, C., Kanbach, G. & Schrey, F., 2001, Exp. Astron. **11**, 157.

[14] Lessard, R.W., *et al.*, 2000, ApJ **531**, 942.

[15] Fortin, P., 2005, Ph.D. Thesis, McGill University.

[16] Oña-Wilhelmi, E. *et al.*, 2004, Astropart. Phys. **22**, 95.

[17] Lucarelli, F. *et al.*, 2005, Proc. 29th ICRC (Pune), **5**, 367.

[18] Bernlöhr, K. *et al.*, 2003, Astropart. Phys. **20**, 111.

[19] Cornils, R. *et al.*, 2003, Astropart. Phys. **20**, 129.

[20] Franzen, A. *et al.*, 2003, Proc. 28th ICRC (Tsukuba), Univ. Academy Press, Tokyo. p. 2987.

[21] Vincent. P. *et al.*, 2003, Proc. 28th ICRC (Tsukuba), Univ. Academy Press, Tokyo. p. 2887.

[22] Funk, S. *et al.*, 2004, Astropart. Phys. **22**, 285.

[23] Jessner, A. *et al.*, 2005, Advances in Space Research, **35**, 1166.

[24] Gillessen, S. 2004, PhD Thesis, University of Heidelberg.

[25] Eifert, T. 2006, Diploma Thesis, Humbolt University, Berlin.

[26] *http://pulsar.princeton.edu/tempo/*

[27] Jodrell Bank pulsar group page, *http://www.jb.man.ac.uk/∼pulsar/*

[28] Percival, J.W., *et al.*, 1993, ApJ **407**, 276.

[29] Preuss, S. *et al.*, 2002, Nucl. Instrum. Meth. A **481**, 229.

[30] Schmidt, F. *et al.*, 2004, 2nd Int. Symp. on High Energy Gamma Ray Astronomy, Heidelberg, APS Conf. Proc. **745**, 377

[31] Hermann, G. *et al.*, 2005, Proc. Cherenkov 2005, Paris (*astro-ph/0511519*).

[32] LeBohec, S., Krennrich, F & Sleege, G. Astropart. Phys. **23**, 235.